Bioconjugate Chemistry

Article

pubs.acs.org/bc

Novel Radiotracer for ImmunoPET Imaging of PD-1 Checkpoint Expression on Tumor Infiltrating Lymphocytes

Arutselvan Natarajan,[†] Aaron T. Mayer,[†,‡] Lingyun Xu,[†] Robert E. Reeves,[†] Jacob Gano,[†] and Sanjiv S. Gambhir*[,†,‡,§]

[†]Radiology, School of Medicine, [‡]Bioengineering and [§]Materials Science and Engineering, Stanford University, Stanford, California 94305, United States

Supporting Information

ABSTRACT: Immune checkpoint signaling through the programmed death 1 (PD-1) axis to its ligand (PD-L1) significantly dampens anti-tumor immune responses. Cancer patients treated with checkpoint inhibitors that block this suppressive signaling have exhibited objective response rates of 20−40% for advanced solid tumors, lymphomas, and malignant melanomas. This represents a tremendous advance in cancer treatment. Unfortunately, all patients do not respond to immune checkpoint blockade. Recent findings suggest that patients with tumor infiltrating lymphocytes (TILs) expressing PD-1 may be most likely to respond to αPD-1/PD-L1 checkpoint inhibitors. There is a compelling need for diagnostic and prognostic imaging tools to assess the PD-1 status of TILs in vivo. Here we have developed a novel immunoPET tracer to image PD-1 expressing TILs in a transgenic mouse model bearing melanoma. A ^{64}Cu labeled anti-mouse antibody (IgG) PD-1 immuno positron emission tomography (PET) tracer was developed to detect PD-1 expressing murine TILs. Quality control of the tracer showed >95% purity by HPLC and >70% immunoreactivity in an in vitro cell binding assay. ImmunoPET scans were performed over 1−48 h on Foxp3+.LuciDTR4 mice bearing B16−F10 melanoma tumors. Mice receiving anti-PD-1 tracer (200 ± 10 μCi/10−12 μg/200 μL) revealed high tracer uptake in lymphoid organs and tumors. BLI images of FoxP3$^+$ CD4$^+$ Tregs known to express PD-1 confirmed lymphocyte infiltration of tumors at the time of PET imaging. Biodistribution measurements performed at 48 h revealed a high (11×) tumor to muscle uptake ratio of the PET tracer ($p < 0.05$). PD-1 tumors exhibited 7.4 ± 0.7%ID/g tracer uptake and showed a 2× fold signal decrease when binding was blocked by unlabeled antibody. To the best of our knowledge this data is the first report to image PD-1 expression *in living subjects* with PET. This radiotracer has the potential to assess the prognostic value of PD-1 in preclinical models of immunotherapy and may ultimately aid in predicting response to therapies targeting immune checkpoints.

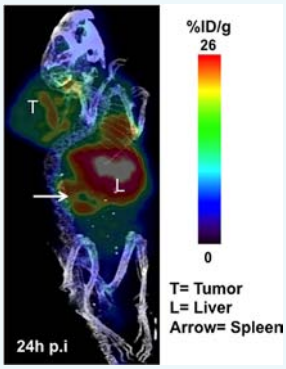

INTRODUCTION

Tumors evade immune surveillance by overexpressing so-called immune checkpoint receptors that serve to negatively regulate T cell effector function.[1,2] While immune checkpoints typically play a key role in maintaining physiologic self-tolerance, tumors have exploited these pathways to evade the anti-tumor immune response by promoting effector T cell inactivation.[3,4] It is becoming clear that signaling through the PD-1 axis significantly dampens anti-tumor immune responses.[3,5−8] PD-1 is a type I transmembrane protein (288 amino acids) and a member of the B7 receptor immunoglobulin family. It is composed of three domains including an immunoglobulin (Ig) superfamily, a transmembrane, and an intracellular domain. The intracellular domain contains approximately 95 residues with an immunoreceptor tyrosine-based inhibitory motif (ITIM) as well as an immunoreceptor tyrosine-based switch motif (ITSM).[8,9] PD-1 is inducibly expressed on lymphocytes including CD4+ and CD8+ effector T cells, natural killer (NK) T cells, B cells, and some dendritic cells.[3,8] Prolonged expression of PD-1 on CD8+ T cells induces exhaustion and loss of effector function.[2,4] Also contributing to the immunosuppressive tumor microenvironment are CD4$^+$Foxp3$^+$ regulatory T cells (Tregs) which are known to express cell surface PD-1.[2,4] PD-1 pathway stimulation therefore results in not only attenuated CD8+ T cell function, but also enhanced Treg activity which creates a strong inhibitory environment in the tumor interstitium. PD-1 has two binding ligands known as PD-L1 and PD-L2. PD-L1 is the primary driver of PD-1 activity and its expression is upregulated by IFN-γ and TNF-α cytokine secretion. PD-L1 is inducibly expressed on most cell types including both hematopoietic and nonhematopoietic lineages to maintain peripheral tolerance; however, pathological expression by tumor cells results in suppression of the anti-tumor immune response.[2,4]

Checkpoint blockade strategies utilizing monoclonal antibody (mAb) antagonists to the PD-1 signaling axis have shown encouraging results in restoring suppressed anti-tumor immunity.[10−23] Several monoclonal antibodies targeted to block PD-1 or its ligand PD-L1 are currently undergoing phase three clinical trials including Nivolumab (Bristol-Myers Squibb, PD-1) and MSB0010718C (Merck, PD-L1), with Pembrolizumab

Received: June 7, 2015
Revised: August 23, 2015
Published: August 26, 2015

DOI: 10.1021/acs.bioconjchem.5b00318
Bioconjugate Chem. 2015, 26, 2062−2069

(Merck, PD-1) having been granted by the FDA fast-track approval for treatment of metastatic melanoma in the United States.[2,10,12,20,24] Even after traditional chemotherapy and radiation therapies have failed, clinical blockade strategies have resulted in an increased prevalence of late-stage patients with progression-free survival beyond the two-year mark, leading some to regard immunotherapy as the new paradigm of cancer treatment.[3] Despite encouraging clinical results, many cancer patients do not respond to clinical checkpoint blockade. While anatomic imaging has been the gold standard to monitor treatment efficacy based upon decreases in tumor size,[25,26] patients treated with immunotherapies often present with a period of apparent tumor growth before prolonged regression.[27] Due to the high cost and delayed response times, there exists a compelling need to accurately predict which patients are most likely to benefit from anti-PD-1/PD-L1 treatment and to establish new assessment criteria.

A number of correlative studies utilizing invasive biopsy in conjunction with immunohistochemistry (IHC) are starting to suggest that PD-1 expression on tumor infiltrating lymphocytes may serve as a good biomarker to predict responders to checkpoint blockade.[28−41] It has been difficult to determine the true prognostic value of PD-1 using these methods, as its expression is highly heterogeneous within both the primary tumor and distant metastases. There is a growing need to investigate the utility of additional, noninvasive methods for detecting and quantifying PD-1 in patients who are candidates for immunotherapies. To date, there are no clinically approved positron emission tomography (PET) tracers available for imaging global PD-1 expression in the context of immune checkpoint therapies. Here we discuss the development of a novel anti-PD-1 immunoPET tracer that is capable of specifically imaging PD-1 expression on TILs and primary lymphoid organs in a transgenic mouse model bearing melanoma.

RESULTS

Preparation of DOTA-anti-mouse-PD-1 mAb. The DOTA-anti-mouse-PD-1 mAb immunoconjugate was prepared by coupling DOTA-NCS to the lysine groups of hamster anti-mouse-PD-1 mAb. We performed three conjugations, in which the best immunoconjugation was achieved by the addition of a 10-fold molar excess of DOTA-NCS over anti-mouse-PD-1 at pH of 7.0, incubated at 37 °C for 45 min. These conditions resulted in a reproducible chelate/PD-1 mAb of 1.5 ± 0.4, confirmed by MALDI-TOF (Supporting Information Figure S1).

Radiolabeling of DOTA-anti-mouse-PD-1 mAb (Figure 1). Radiolabeling of DOTA-anti-mouse-PD-1 mAb with ^{64}Cu in 0.1 M ammonium acetate buffer (pH 5.3) yielded greater than 80.4 ± 6.8% (mean ± SD) with specific activity of 0.7 ± 0.1 MBq/μg. The highest radiochemical yield achieved was 87% at 37 °C, of pH 7.0, at incubation for 60 min. Table 1 shows the quality assurance of the ^{64}Cu-DOTA-PD-1 PET tracer. Figure 1 demonstrates the radiochemical purity of the tracer (mean ± STD: 98.0 ± 1.8%) determined by SEC 3000-HPLC.

Ex Vivo Cell Binding Study (FACS Assay) (Figure 2). Figure 2 shows the binding affinity of the DOTA-anti-mouse-PD-1 tracer tested on ex vivo mouse splenic cells (with and without Concanavalin A induced expression of PD1). Compared to the unstimulated control splenic cells (dotted histogram), and isotype control antibody (open histogram), DOTA-anti-mouse-PD-1 (filled histogram) exhibits high binding efficiency to the PD-1 receptor expressed on induced splenocytes. The results of the binding assay (Figure 2) indicate that the conjugate was able to bind specifically to PD-1 protein expressed on splenocytes. PD-1 binding was also confirmed on PD-1 overexpressing CT 26 cells. The immunoreactivity of the ^{64}Cu-DOTA-PD-1 PET tracer was calculated to be 76 ± 4.6% (Supporting Information Figure S2).

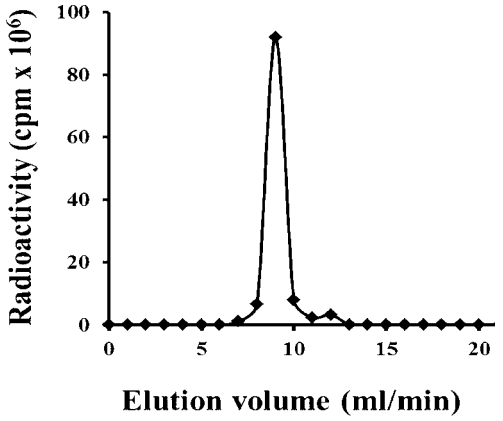

Figure 1. Radio-HPLC. Radio-HPLC chromatogram of the PET tracer shows the purity of the ^{64}Cu-DOTA-anti-mouse-PD-1 tracer. The PET tracer was eluted by SEC 3000 column at a flow rate of 1 mL/min using PBS. Radioactivity of each of the 1 mL fractions was collected and counted in gamma counter as counts per minute (cpm).

Table 1. Quality Control Performed on ^{64}Cu-DOTA-anti-mouse-PD1 ImmunoPET Tracer

immunoPET tracer specifications	results
chemical purity (HPLC)	>98%
chelates/antibody (c/a)	1.5 ± 0.4
pH	6.5−7.5
radiochemical purity (TLC/HPLC)	>95%
radiolabeling yield	80.4 ± 6.8
specific activity	105.4 ± 14.7 GBq/μmol (0.7 ± 0.1 MBq/μg)
immunoreactivity	>70%

Melanoma Xenograft BLI Imaging for Tregs (Figure 3). In Figure 3A we have shown BLI images of Foxp3+.LuciDTR4 Treg cells homing to the subcutaneous tumor. Figure 3B depicts ex vivo organs from Foxp3+.LuciDTR4 mice clearly indicating the homing of Tregs to the tumor as well as the spleen.

Tregs are known to express PD-1 and contribute to the suppression of anti-tumor immunity. Originally this model was created by Hammerling et al., to show that Treg depletion is critical for activation and enhanced infiltration of tumor specific CD8+ T cells leading to tumor immune rejection.[42] This group has shown that localization of Tregs within the tumor microenvironment is often accompanied by the presence of other TILs. These other TILs and invading cell subtypes potentially include CD4+ and CD8+ T cells, natural killer (NK) T cells and certain dendritic cells that are all known to inducibly express PD-1.[2] Many of these cell subtypes first have PD-1 expression activated in the spleen where dendritic cells scavenge particulate antigens and present them on MHC receptors priming antigen specific immune responses. Although PD-1 has been predominantly characterized in T cells, it is also known to be expressed on B cells during differentiation and upregulated in mature B cells following stimulation with TLR9 agonists which can occur in B cell rich zones and germinal centers of the spleen.[2] BLI images of Treg homing and localization thus confirmed that TILs were present in the tumor interstitium and spleen at the time of PET imaging.

DOI: 10.1021/acs.bioconjchem.5b00318
Bioconjugate Chem. 2015, 26, 2062−2069

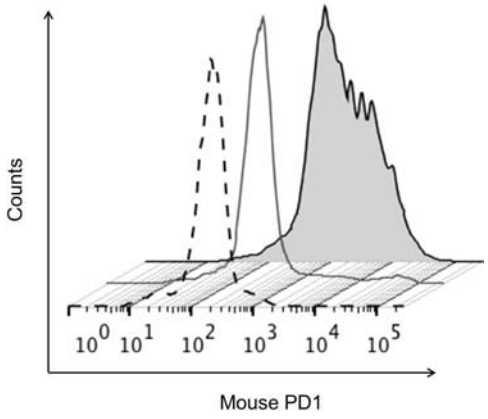

Figure 2. FACS live cell binding assay for the determination of binding specificity of DOTA-PD-1. Flow cytometry analysis of mouse PD-1 expression on ex vivo mouse splenocytes. Cells (1×10^6) were stained with DOTA-hamster-anti-mouse PD-1 mAb or isotype control Hamster-IgG, followed by anti-hamster-IgG-APC. Histogram traces correspond to noninduced cell control (dotted histogram), and cells induced to express PD-1 with Con A (0.5 μg/μL in 100 μL for 2 h) stained with either IgG Isotype control (open histogram) or anti-mouse PD1 (filled histogram).

Small Animal PET and CT Imaging (Figures 4–6). The anti-mouse PD-1 tracer exhibited binding on PD-1 expressing lymphocytes. PET scans were performed at various time points (1–48 h) post injection of 7–8 MBq of ^{64}Cu-DOTA-PD-1 (10–12 μg of anti-mouse PD-1 antibody). PET images shown are coregistered with CT for anatomical delineation. Figures 4–6 show that the immunoPET tracer uptake was at the expected sites of murine PD-1 expression in Foxp3+.LuciDTR4 mice bearing B16F10 mouse melanoma xenografts including the tumor and spleen.

Imaging was also performed in blocking cohorts of PD-1 by preadministration of cold anti-mouse-PD-1 monoclonal antibody. Representative coronal immunoPET images of mice bearing melanoma using the ^{64}Cu-DOTA-PD-1 tracer at various time points are shown in Figure 4. These PET-CT images were obtained at 1, 4, 18, and 24 h post injection of tracer. In Figure 5, we have shown the results of ROI quantification analysis performed on PET-CT images. Figure 6 illustrates PET-CT images obtained after 48 h post injection along with control mice (blocking = preblocked with 5-fold excess cold anti-mouse-PD-1 mAb over tracer mass 2 h prior to tracer injection). From these images it is evident that ^{64}Cu-DOTA-PD-1 tracer had PD-1 specific uptake in the tumor and lymphoid associated organs. The tracer exhibited excellent tumor-to-background (muscle) contrast at all time points from 1 to 48 h.

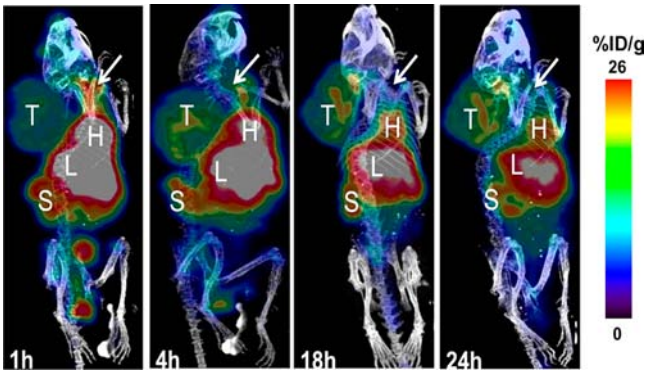

Figure 4. PET/CT images over 24 h. ImmunoPET images of maximum intensity projections (MIP) show Foxp3.Lu-DTR4 transgenic mice bearing melanoma (B16F10) tumors. Each mouse received ^{64}Cu-DOTA-anti-mouse PD-1 tracer. PET/CT images were acquired for 3–10 min at 1, 4, 18, and 24 h post tracer injection (7.4 ± 0.4 MBq/10–12 μg of anti-mouse-PD1). White Arrow = Thymus or Lymph Nodes, L = Liver, T = Tumor, H = Heart, S = Spleen. Scale bar represents %ID/g with red-shifted regions indicating high uptake and blue-shifted regions indicating low uptake.

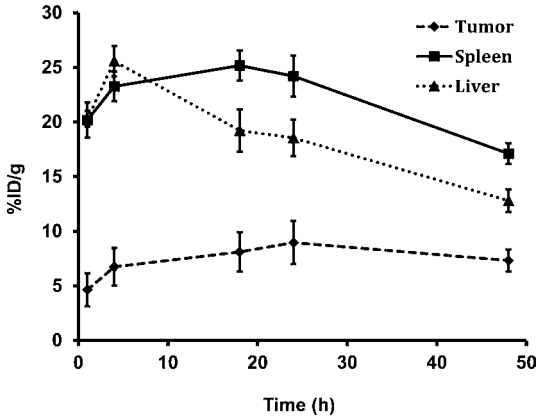

Figure 5. ROI analysis over 48 h. Tumor and spleen uptake was estimated from the ROI of PET-CT images exhibited in Figure 4 and Figure 6. The *Y*-axis is %ID/gram and *X*-axis indicates PET scan time post injection.

Biodistribution Studies of Tumor-Bearing Mice (Table 2, Figure 7). The biodistribution results at 48 h post

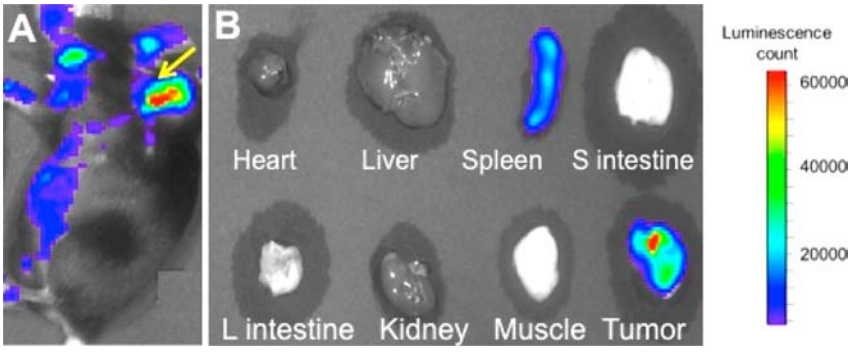

Figure 3. BLI Imaging. BLI and PET/CT images of Foxp3+.Lu-DTR4 transgenic mice. (A) Bioluminescence-based optical (BL) image (5 min after 4 mg of D-luciferin dose by IP, 1 min scan) of Tregs homing to tumor in DTR4 transgenic mouse bearing melanoma tumor. Yellow arrow = tumor (16th day post implantation). (B) BLI images of the ex vivo mouse organs. Organs were dissected and kept in 200 μL of D-luciferin for 1 min and scanned for BL for 30 s image.

DOI: 10.1021/acs.bioconjchem.5b00318
Bioconjugate Chem. 2015, 26, 2062–2069

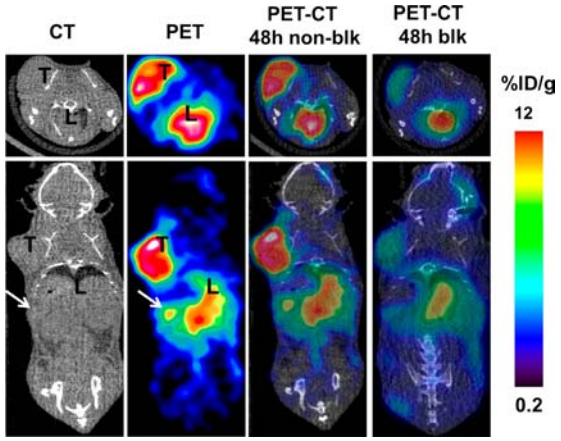

Figure 6. PET-CT images of a tumor-bearing mouse at 48 h of anti-PD1 tracer [64-Cu-DOTA-mPD-1 IgG antibody; 200 ± 10 μCi/10 ± 2 μg/200 μL] signal with and without blocking. T = Tumor; L= Liver; White Arrow = Spleen. Scale bar represents %ID/g with red-shifted regions indicating high uptake and blue-shifted regions indicating low uptake.

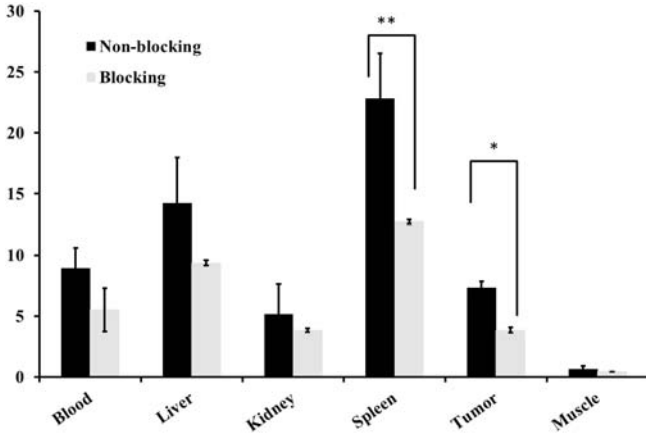

Figure 7. Histogram shows ^{64}Cu-DOTA-mPD1 tracer biodistribution in melanoma xenografted DTR transgenic mice (2 groups) after 48 h post injection. Mice (blocked) (n = 3) received 2 mg/kg predose of unconjugated anti-mouse PD1 antibody 2 h before tracer injection (i.v., dose 7.4 ± 0.4 MBq). The nonblocked mice (n = 4) received no predose. Organ uptake of tracer dose was measured (mean %ID/g ± SD) after 48 h post injection by the γ counter. %ID/g of tissue was decay corrected. Tracer uptake in nonblocking tumor is 2-fold higher than blocking cohorts. Further, the tracer uptake value in spleen is significantly higher when compared to tumor, liver, and kidney. As expected, this data indicates that the tumor and spleen are the major organs containing PD-1 expressing lymphocytes. P* <0.05, ** <0.1.

injection (Figure 7) correlated to the PET ROI quantification results in Figure 5. The ^{64}Cu-DOTA-PD-1 tracer uptake by TILs in nonblocking and blocking mice was (mean % ID/g ± SD) 7.4 ± 0.71 and 4.51 ± 0.26, respectively. The tracer tumor-to-tissue uptake ratios in nonblocking mice for tumor-to-blood and tumor-to-muscle are 0.8 and 11.0, respectively (P < 0.05). The tracer uptake (%ID/g ± SD) in clearance organs such as liver and kidney are 16.09 ± 3.72 and 5.61 ± 3.37 at 48 h.

DISCUSSION

Immune checkpoint inhibitors are showing incredible translational promise. Recently, the FDA has approved several immunotherapy drugs with others in ongoing clinical trials such as

Table 2. Biodistribution Data of the Tracer in Tumor Bearing Mice

	24 h	48 h blocking	48 h nonblocking
organs	mean (%ID/g) ± SD	mean (%ID/g) ± SD	mean (%ID/g) ± SD
blood	16.04 ± 0.43	6.4 ± 2.05	8.55 ± 2.24
heart	3.85 ± 0.31	2.74 ± 0.52	3 ± 0.95
lungs	5.4 ± 1.82	4.22 ± 0.18	5.45 ± 1.53
liver	19.5 ± 0.51	10.73 ± 0.27	16.09 ± 3.72
spleen	27.67 ± 0.02	14.39 ± 0.53	23.04 ± 4.97
thymus	3.62 ± 1.02	3.04 ± 0.97	3.81 ± 0.34
pancreas	1.81 ± 0.03	1.06 ± 0.12	2.17 ± 0.48
stomach	3.62 ± 0.23	1.81 ± 0.45	2.24 ± 0.2
small intestine	6.4 ± 0.19	2.23 ± 0.22	5.41 ± 1.32
large intestine	7.71 ± 2.38	2.39 ± 0.22	5.57 ± 1.92
kidney	8.39 ± 0.67	4.52 ± 0.25	5.61 ± 3.37
muscle	0.67 ± 0.03	0.55 ± 0.05	0.69 ± 0.31
bone	2.44 ± 0.93	1.44 ± 0.06	1.78 ± 1
bone marrow	0.15 ± 0.08	0.23 ± 0.02	0.18 ± 0.15
brain	0.68 ± 0.04	0.27 ± 0.03	0.46 ± 0.08
skin	1.64 ± 0.04	1.19 ± 0.48	1.75 ± 1.29
tumor	9.37 ± 0.09	4.51 ± 0.26	7.4 ± 0.71

Nivolumab (anti-PD-1 human IgG4 mAb by Bristol-Myers Squibb), MPDL3280A (anti-PD-L1 human IgG mAb by Roche[20]), and Pembrolizumab (anti-PD-1 IgG4 by Merck). Blockade of checkpoint receptor or ligand pathways has proven to enhance effector T-cell infiltration, activation, and effector function in the tumor microenvironment.[14,32] Understanding the events that take place in generating and regulating anti-tumor immunity is essential to the development and improvement of therapeutic strategies. It is not currently known why only a certain subset of patients respond to these therapies, but hypotheses include lack of PD-1/PD-L1 checkpoint expression or that resistant cancer cells may be exploiting other immune checkpoint associated pathways such as CTLA-4, TIM-3, BTLA, and VISTA. It remains unclear whether the effector function of tumor infiltrating lymphocytes (TILs) can be restored by targeting a single receptor and combinatorial checkpoint blockade may be required for sustained immune activation.[3] For example, Ipilimumab (anti-CTLA4) and Nivolumab (ant-PD-1) are being investigated under FDA fast track in combination against melanoma. Several preliminary studies have indicated that blockade of both PD-1 and CTLA-4 pathways have synergistic effects and results in enhanced activation of tumor antigen specific CD8+ cytotoxic and CD4+ helper T cells.[18,36]

As we seek to better understand immune checkpoint mechanisms of action and improve therapeutic response, there remains an explicit need for tools that can monitor and predict responders to anti-PD-1 immunotherapy. Currently, immunohistochemical staining and scoring is the only tool available to measure and evaluate PD-1/PD-L1 expression.[14,32] This technique suffers from several limitations including the need for invasive biopsy, inadequate sampling of the highly heterogeneous primary tumor, and lack of information about expression profiles of metastatic lesions. Furthermore, this technique is not feasible for some tumors that are inaccessible for biopsy. PET imaging provides an ideal alternative that allows for noninvasive, dynamic monitoring and overall evaluation of checkpoint receptor expression.

In this report we have shown effective preclinical imaging of PD-1 expressing TILs in a melanoma tumor model utilizing

DOI: 10.1021/acs.bioconjchem.5b00318
Bioconjugate Chem. 2015, 26, 2062−2069

a novel anti-PD-1 immunoPET radiotracer (Figures 4−6). The anti-PD-1 mAb was conjugated to DOTA-NCS and MALDI-TOF mass spectrometry confirmed 1−2 chelates per antibody (Figure S1). The radiotracer was successfully synthesized with greater than 95% radiochemical purity and high specific activity (Table 1). Prior to performing the preclinical studies, in vitro live cell binding assays were performed, which demonstrated high immunoreactivity (>70%, Table 1, Figure 2, and Figure S2). These cell binding assays help to show the specificity of the tracer for PD-1 expression. In the FACS study (Figure 2), the DOTA conjugated anti-PD1 mAb showed high specificity for the intended PD-1 target, when compared to both isotype control mAb and our negative control cells, which were not induced to express PD-1. The ^{64}Cu-DOTA-PD-1 tracer was then used in a followup cell assay indicating that radiolabeling did not negatively affect the immunoreactive fraction (0.71, Figure S2). After the successful synthesis and in vitro specificity of our tracer confirmed, we then tested our tracer in an in vivo preclinical model of Foxp3+.LuciDTR4 mice bearing B16F10 mouse melanoma xenografts. The advantage of this model is that FoxP3+ Treg cells reported in the literature to highly express PD-1 and play an important role in regulating the immunosuppressive tumor microenvironment have been engineered to express luciferase. BLI confirmed the presence of tumor infiltrating lymphocytes known to express PD-1 (Tregs) at the time of PET imaging.

To further validate the expression of our target (PD-1) in the tumor microenvironment, we performed both Western blot and IHC-IF (Figures S3−4). The Western blot data clearly indicated that PD-1 was expressed in both spleen and tumor tissues while the PD-L1 protein was expressed in tumor tissue alone. The immunofluorescence results clearly show that PD-1 is being expressed in the tumor correlating well with our confirmation of the presence of TILs known to express PD-1 (Treg) by BLI imaging. Once again this staining was highly specific when compared to liver, which should not express high amounts of PD-1 and isotype controls. Upon injection of the radiotracer, our results show moderate to high tracer uptake in the tumor and spleen. The spleen plays an important role in priming T cells before deploying them throughout the body for antigen surveillance and attack. The signals coming from the tumors are lymphocytes that have homed to and infiltrated the tumor. The immunosuppressive tumor microenvironment is thought to play a role in the up regulation of PD-1 expression on these TILs resulting in CD8+ cytotoxic T cell anergy and loss of effector function.

The PET imaging analysis suggests that we are able to specifically image PD-1 expression in the tumor and spleen. Blocking studies illustrate the in vivo specificity of the tracer, with a cold dose preinjection of mAb before radiotracer imaging effectively decreasing the signal from PD-1 expressing lymphocytes in both the tumor and spleen, while other organs such as muscle exhibit nonsignificant changes in signal intensity between blocking and nonblocking groups. The liver and kidney show slightly decreased signal in the blocking group, but these differences are not statistically significant and the high variability in these measurements can be accounted for by the fact that these are clearance organs. We believe further optimization of the ^{64}Cu-DOTA-PD-1 radiotracer could be achieved through dose optimization and alternative chelation strategies and these pose compelling areas for future exploration. The fact that the ^{64}Cu-DOTA-PD-1 radiotracer signal could be blocked with just a 5-fold higher dose of cold antibody suggests that a lower dose may be feasible for imaging. Taken as a whole, the data presented here illustrates the successful development of a novel PD-1 imaging probe.

PD-1 expression may be a very useful biomarker of response to anti-PD-1/PD-L1 therapies. Future work will seek to correlate PD-1 expression levels to the PET signal. This tool could be useful in evaluating the true prognostic value of PD-1 expression in preclinical models. Although this tool is currently limited to imaging the expression of murine PD-1, this study has provided insight[18,43,44] and proof-of-concept for the future development[39,45] of an optimized anti-PD1-human tracer that could eventually help predict responders to immune checkpoint blockade in the clinic. The radiotracer described here exhibits many favorable imaging characteristics, but a current drawback is the high background signal in blood even at 48 h post injection. Future studies should explore the development of small protein tracers such as scFvs and fibronectin type 3 domains, which are known to have advantages for imaging including faster clearance and enhanced tumor penetration.

Despite these current limitations, here we have developed a novel immunoPET tracer that specifically targets PD-1 expressing TILs and lymphoid organs in a Foxp3+DTR4 transgenic mouse xenograft bearing melanoma. The approach we have described could allow for noninvasive imaging and measurement of PD-1 immune checkpoint expression before and during immunotherapy, providing valuable opportunities to monitor and assess checkpoint blockade strategies.

EXPERIMENTAL SECTION

Reagents, Antibodies, and Radiochemicals. All reagents were obtained from Sigma-Aldrich (St. Louis, MO) unless otherwise stated. The 2-(4-isothiocyanatobenzyl)-1,4,7,10-tetraazacyclododecane-1,4,7,10-tetraacetic (DOTA-NCS) were purchased from Macrocyclics (Dallas, TX, USA). $^{64}CuCl_2$ ($t_{1/2}$ = 12.7 h, radionuclide purity >99%; 2−3 GBq/mL in 0.1 M hydrochloric acid) was obtained from the University of Wisconsin (Madison, WI, USA). The mAb (0.5 mg/mL) directed against mouse PD-1 was purchased from Affymetrix eBioscience (San Diego, CA, USA). It is a high-affinity monoclonal antibody raised in hamster and functional grade purified (clone J43).

Cell Lines and Instruments. The murine PD-1 expressing cell line was developed in-house from the CT 26 (mouse colon cancer) American Type Culture Collection (www.atcc.com, ATCC number: CRL-2638) transfected with pC Puro Ubx mPD1-IRES-eGFP cDNA and Lipofectamine 3000. The transfected cells were incubated with 5 ng/mL of Puromycin in RPMI media for several days for GFP positive cell selection. FACS was performed with EGFP signal to enrich mPD1 positive cells (two times). CT26 cells were maintained in Dulbecco's modified Eagle's medium (DMEM) (4.5 g/L glucose). All media was supplemented with 10% fetal calf serum (FCS), 2 mmol/L glutamine, 100 units/mL penicillin, 100 μg streptomycin, and 0.25 μg/mL fungizone. All media and additives were obtained from Invitrogen Corporation (Carlsbad, CA USA).

Mouse melanoma B16−F10 (ATCC CRL-6475) cell line was purchased from ATCC. High-performance liquid chromatography (HPLC) was performed on an HPLC-Ultimate 3000 with a SEC 3000 LC column (300 × 7.8 mm) with 5 μm, hydrophilic bonded silica support, of 400-Å pore size (Phenomenex, Torrance, CA 90501−1430, USA) with an ultraviolet detector and an online radioactivity detector. Mass spectrometry (AB SCIEX TOF/TOF 5800) was performed at Stanford University and operated in linear mode with sinapinic acid as the matrix.

DOI: 10.1021/acs.bioconjchem.5b00318
Bioconjugate Chem. 2015, 26, 2062−2069

Preparation of Immunoconjugate and ImmunoPET Tracer. DOTA-anti-mouse-PD-1-mAb was prepared by conjugating DOTA-NCS to anti-PD1-mAb. DOTA-NCS is well-known to chelate 64-Cu. Briefly, anti-PD1-mAb was purified by Phenomenex size-exclusion chromatography (SEC) 3000 (Torrance, CA, USA) HPLC with 0.1 M sodium phosphate buffer (pH 7) at 1 mL/min and concentrated to ∼1.5 mg mL^{-1} using an Amicon 30 kDa centrifugal Ultra-2 filter. This concentrated anti-PD1-mAb solution (10 nmol, 1 mL, 0.01 mM) was then mixed with 80% DMSO in water solution of DOTA-NCS (100 nmol, 0.005 mL, 20 mM). The pH of the reaction mixture was adjusted to 8.5−9.0 and incubated for 45 min at 37 °C. DOTA-anti-PD-1-mAb was purified from excess DOTA-NCS by SEC3000 HPLC using 0.1 M ammonium acetate buffer (pH 5.5) as the mobile phase eluted at 1 mL/min. The immunoconjugates were concentrated to ∼1 mg/mL using an Amicon 30 kDa centrifugal filter and stored in 200 μL aliquots in 0.1 M ammonium acetate buffer (pH 5.5) at −20 °C. The number of chelators (c) coupled per antibody (a), i.e., c/a was estimated with matrix-assisted laser desorption/ionization time-of-flight mass spectrometry (MALDI-TOF-MS) by comparison of anti-PD-1-mAb and DOTA-anti-PD-1-mAb.[33]

In Vitro Live Cell Binding Assay of DOTA-anti-PD-1-mAb. Prior to radiolabeling, immunoreactivity of the DOTA-anti-PD-1-mAb was tested on ex vivo mouse splenic cells and analyzed by flow cytometry. Briefly, DOTA-anti-PD-1-mAb and unmodified anti-PD-1 were diluted to 500 μL ranging from 50 μg/mL to 390 ng/mL in FACS buffer Dulbecco's PBS with 2% FCS and 0.1% sodium azide. Staining was performed in 96-well microtiter plates (V-bottom). In each well 100 μL of the antibody was mixed with 50 μL cell suspension containing 5×10^5 splenic cells and incubated for 1 h on ice. Cells were washed three times with FACS buffer, followed by each well receiving 100 μL of anti-hamster IgG/Fc-FITC (eBioscience, Inc., San Diego, CA) prediluted to 1:100 in FACS-buffer. The plate was incubated for 30 min on ice in the dark and cells were washed three times. Dead cells were discriminated by propidium iodide staining. Analysis was carried out on a flow cytometer (FACS Aria III, BD Biosciences, San Jose, CA, USA) at the Stanford FACS Facility. Data was analyzed by FlowJo FACS analysis software (Tree Star, Ashland, OR, USA).

Radiolabeling of ImmunoPET Tracer. To achieve high specific activity and radiochemical yield, the labeling reaction was performed in a 1.5 mL Eppendorf tube in the following sequence: ^{64}Cu (220−230 MBq; 500 μL), 0.1 M ammonium acetate buffer (200 μL, pH 5.4), and DOTA-anti-PD-1-mAb (300 μL, 300 μg) were added. After incubation (45 min), 0.1 M ethylenediaminetetraacetic acid (EDTA), pH 7.0, was added to achieve final concentration of 10 mM for 15 min to scavenge unchelated ^{64}Cu in the reaction mixture.

Purification of the radioimmunoconjugate (300 μg in 1100 μL volume) was achieved by SEC-3000 column in PBS buffer [0.1 mol/L NaCl, 0.05 mol/L sodium phosphate (pH 7.4)] at a flow rate of 1.0 mL/min. The radioimmunoconjugate peak (retention time at 8.5 min) corresponding to antibody was collected and concentrated using an Amicon Ultra-15 (Millipore, USA) device, and centrifuged at 3000g for 15 min. The final product was filtered through a 0.2 μm filter into a sterile vial.

Quality Assessment of the ImmunoPET Tracer. The ^{64}Cu-DOTA-anti-PD-1-mAb radiochemical purity was analyzed by thin layer chromatography, as well as SEC 3000 radio-HPLC. Immunoreactivity of the immunoPET tracer was assayed by live cell-binding assays as described by previous publications.[46,47] Briefly, PD-1 (PD-1 +) and CT 26 (eGFP expressing) cells were suspended in microcentrifuge tubes at concentrations of 5.0 to 0.08×10^6 cells/mL (2-fold dilutions; six concentrations) in 500 μL PBS (pH 7.4). Aliquots of ^{64}Cu-DOTA-anti-PD-1-mAb (250 μL of a stock solution of 0.37 MBq, [0.01 mCi] in 10 mL of 1% bovine serum albumin [BSA]; [0.25 μCi], 0.01 μg of mAb) were added to each tube (n = 2; final volume: 750 μL). After addition of tracer, the solutions were gently vortexed and incubated at 37 °C. Two hours later the solutions were centrifuged (300g for 5 min), resuspended, and washed twice with ice-cold PBS before removing the supernatant. Cells were then pelleted by centrifugation and counting was performed for the ^{64}Cu-activity associated with the cell pellet. The activity was counted in a γ-counter (1470 WIZARD Automatic Gamma Counter; PerkinElmer, Walthem, MA). The count data were background corrected and compared with the total number of counts in control samples. Competitive inhibition (blocking) assays were conducted by using the same procedure but with the addition of unmodified anti-PD-1-mAb (50 μL, 0.2 mg/mL in 1% BSA, [1000-fold excess mAb; 10 μg]) to the ^{64}Cu-DOTA-anti-PD-1-mAb solutions.

Animal Studies. Animal studies were performed in compliance with approval from the Administrative Panel on Laboratory Animal Care (APLAC) at Stanford University. The Treg+ transgenic mice (Foxp3+.LuciDTR) were obtained from Dr. Hammerling's lab for the experiments.[42] Prior to the animal study, Treg+ transgenic mice were screened to confirm the expression of Treg+ positive targets by reverse transcription polymerase chain reaction (RT-PCR). The average weight of the mice was 25.0 ± 2.0 g. Two groups of transgenic mice (blocking and nonblocking) and nude/nude mice (negative control) (4 animals for each group) were imaged at 1, 4, 18, 24, and 48 h using small animal PET at the Stanford small animal imaging center. All experimental mice received ^{64}Cu-labeled radiopharmaceutical [200 μL, corresponding to 7.4 ± 0.4 MBq, 10−12 μg of DOTA-anti-PD-1-mab] via tail vein injection. After radiotracer administration, the animals were scanned at the time points indicated above. Results are reported as % injected dose per gram of tissue (%ID/g). Statistical analysis was done with Student's t test (two-tailed, unequal variance).

Small Animal ImmunoPET-CT Imaging. To acquire the PET-CT images the ^{64}Cu-DOTA-PD-1 radiotracer (7.4 ± 0.4 MBq dose) was administered to lightly restrained Treg+ transgenic mice via a lateral tail vein. PET-CT imaging was performed on a Siemens Inveon small-animal multimodality PET/CT system (Preclinical Solutions; Siemens Healthcare Molecular Imaging, Knoxville, TN). This system is capable of operating both the PET and CT scanners independently or in combination with excellent radial, tangential, and axial resolutions higher than 1.5 mm at the center of the field of view of the PET module. CT imaging was performed at 80 kVp at 500 μA, second bed position, half scan 220° of rotation, and 120 projections per bed position with a cone beam micro-X-ray source (50 μm focal spot size) and a 4064 × 4064 pixel X-ray detector. The data was reconstructed using Shepp-Logan filtering and cone-beam filtered back-projection.

The micro PET scanning [default settings of coincidence timing window of 3.4 ns and energy window of 350 to 650 keV] was performed at the following time points after the tracer injection: 1 h for 3 min; 4 and 18 h for10 min; 24 and 48 h for 15 min scans. The images acquired were reconstructed with two-dimensional ordered-subset expectation maximization (OSEM 2D) algorithm.[46] PET-CT images and three-dimensional regions

DOI: 10.1021/acs.bioconjchem.5b00318
Bioconjugate Chem. 2015, 26, 2062−2069

of interest (ROI) of organs of interest were computed using Inveon Research Workplace software (Preclinical Solutions; Siemens Healthcare Molecular Imaging, Knoxville, TN). The mean pixel values within the ROI volume was converted to radioactivity concentration in counts per milliliter per minute (cpm) by using a predetermined conversion factor. The percentage-injected dose per gram of tissue (%ID/g) was estimated by dividing each tissue's cpm obtained from the region of interest by the injected dose. At each time point before imaging, animals were anesthetized and scanned at the same conditions as detailed above.

Biodistribution Study of ^{64}Cu-DOTA-anti-PD-1-mAb. In vivo biodistribution studies were performed to evaluate the uptake of ^{64}Cu-DOTA-anti-PD-1-mAb in Treg+ transgenic mice at 24 and 48 h post injection. Mice (n = 5, per group) with blocking (received 2 mg/kg cold dose of DOTA-anti-PD-1-mAb 2 h prior to tracer injection) and nonblocking (tracer alone) received ^{64}Cu-DOTA-anti-PD-1-mAb [200 μL, corresponding to 7.4 ± 0.4 MBq, 10−12 μg of DOTA-anti-PD-1-mAb, via intravenous (i.v.) tail-vein injection (t = 0 h). Animals were euthanized by CO2 gas asphyxiation at 24 and 48 h postinjection and organs were removed, rinsed in PBS, dried in air for 5 min, weighed, and counted in a gamma-counter for ^{64}Cu-activity. The ^{64}Cu-DOTA-anti-PD-1-mAb dose uptake by each organ was determined by measuring the total number of counts (counts per minute, [cpm]). Count data were background subtracted and decay corrected at the time of injection and the percent-injected dose per gram (%ID/g) for each tissue sample was calculated by normalization to the total activity injected.

Statistical Analysis. Unpaired Student's t-test was used for data comparisons. P values less than 0.05 were considered statistically significant.

■ ASSOCIATED CONTENT

Supporting Information

The Supporting Information is available free of charge on the ACS Publications website at DOI: 10.1021/acs.bioconjchem.5b00318.

MALDI; in vitro live cell binding assay; Western blot analysis; immunofluorescent detection of PD-1 expression on TILs; materials and methods (PDF)

Movie of ^{64}Cu-DOTA-anti-PD-1-mab immunoPET tracer in a melanoma mouse (MPG)

■ AUTHOR INFORMATION

Corresponding Author

*E-mail: sgambhir@stanford.edu. Phone: 650-725-2309. Fax: 650-724-4948.

Notes

The authors declare no competing financial interest.

■ ACKNOWLEDGMENTS

We acknowledge the support of Drs. Günter J. Hammerling, Mark Stolowitz, Timothy Doyle, Frezghi Habte, Sindhuja Ramakrishnan, the Canary Foundation, the Ben and Catherine Ivy Foundation, and the National Cancer Institute grants ICMIC P50CA114747 (S.S.G.). MicroPET/CT imaging and Gamma Counter measurements were performed in the SCi^3 Stanford Small Animal Imaging Service Center.

■ REFERENCES

(1) Nguyen, L. T., and Ohashi, P. S. (2014) Clinical blockade of PD1 and LAG3–potential mechanisms of action. *Nat. Rev. Immunol. 15*, 45−56.

(2) Ohaegbulam, K. C., Assal, A., Lazar-Molnar, E., Yao, Y., and Zang, X. (2015) Human cancer immunotherapy with antibodies to the PD-1 and PD-L1 pathway. *Trends Mol. Med. 21*, 24−33.

(3) Mellman, I., Coukos, G., and Dranoff, G. (2011) Cancer immunotherapy comes of age. *Nature 480*, 480−9.

(4) Rosenberg, S. A. (2004) Development of effective immunotherapy for the treatment of patients with cancer. *Journal of the American College of Surgeons 198*, 685−96.

(5) Drake, C. G., Jaffee, E., and Pardoll, D. M. (2006) Mechanisms of immune evasion by tumors. *Adv. Immunol. 90*, 51−81.

(6) Fridman, W. H., Pages, F., Sautes-Fridman, C., and Galon, J. (2012) The immune contexture in human tumours: impact on clinical outcome. *Nat. Rev. Cancer 12*, 298−306.

(7) Mullard, A. (2013) New checkpoint inhibitors ride the immunotherapy tsunami. *Nat. Rev. Drug Discovery 12*, 489−92.

(8) Agata, Y., Kawasaki, A., Nishimura, H., Ishida, Y., Tsubat, T., Yagita, H., and Honjo, T. (1996) Expression of the PD-1 antigen on the surface of stimulated mouse T and B lymphocytes. *Int. Immunol. 8*, 765−72.

(9) Zou, W., and Chen, L. (2008) Inhibitory B7-family molecules in the tumour microenvironment. *Nat. Rev. Immunol. 8*, 467−477.

(10) Topalian, S. L., Sznol, M., McDermott, D. F., Kluger, H. M., Carvajal, R. D., Sharfman, W. H., Brahmer, J. R., Lawrence, D. P., Atkins, M. B., Powderly, J. D., et al. (2014) Survival, durable tumor remission, and long-term safety in patients with advanced melanoma receiving nivolumab. *J. Clin. Oncol. 32*, 1020−30.

(11) Weber, J. S., Kudchadkar, R. R., Yu, B., Gallenstein, D., Horak, C. E., Inzunza, H. D., Zhao, X., Martinez, A. J., Wang, W., Gibney, G., et al. (2013) Safety, efficacy, and biomarkers of nivolumab with vaccine in ipilimumab-refractory or -naive melanoma. *J. Clin. Oncol. 31*, 4311−8.

(12) Wolchok, J. D., Kluger, H., Callahan, M. K., Postow, M. A., Rizvi, N. A., Lesokhin, A. M., Segal, N. H., Ariyan, C. E., Gordon, R. A., Reed, K., et al. (2013) Nivolumab plus ipilimumab in advanced melanoma. *N. Engl. J. Med. 369*, 122−33.

(13) Barber, D. L., Wherry, E. J., Masopust, D., Zhu, B., Allison, J. P., Sharpe, A. H., Freeman, G. J., and Ahmed, R. (2006) Restoring function in exhausted CD8 T cells during chronic viral infection. *Nature 439*, 682−7.

(14) Berghoff, A. S., Ricken, G., Widhalm, G., Rajky, O., Hainfellner, J. A., Birner, P., Raderer, M., and Preusser, M. (2014) PD1 (CD279) and PD-L1 (CD274, B7H1) expression in primary central nervous system lymphomas (PCNSL). *Clinical neuropathology 33*, 42−9.

(15) Brown, J. A., Dorfman, D. M., Ma, F. R., Sullivan, E. L., Munoz, O., Wood, C. R., Greenfield, E. A., and Freeman, G. J. (2003) Blockade of programmed death-1 ligands on dendritic cells enhances T cell activation and cytokine production. *J. Immunol. 170*, 1257−66.

(16) Curran, M. A., Montalvo, W., Yagita, H., and Allison, J. P. (2010) PD-1 and CTLA-4 combination blockade expands infiltrating T cells and reduces regulatory T and myeloid cells within B16 melanoma tumors. *Proc. Natl. Acad. Sci. U. S. A. 107*, 4275−80.

(17) Dong, H., Strome, S. E., Salomao, D. R., Tamura, H., Hirano, F., Flies, D. B., Roche, P. C., Lu, J., Zhu, G., Tamada, K., et al. (2002) Tumor-associated B7-H1 promotes T-cell apoptosis: a potential mechanism of immune evasion. *Nat. Med. 8*, 793−800.

(18) Franceschini, D., Paroli, M., Francavilla, V., Videtta, M., Morrone, S., Labbadia, G., Cerino, A., Mondelli, M. U., and Barnaba, V. (2009) PD-L1 negatively regulates CD4+CD25+Foxp3+ Tregs by limiting STAT-5 phosphorylation in patients chronically infected with HCV. *J. Clin. Invest. 119*, 551−64.

(19) Hamanishi, J., Mandai, M., Iwasaki, M., Okazaki, T., Tanaka, Y., Yamaguchi, K., Higuchi, T., Yagi, H., Takakura, K., Minato, N., et al. (2007) Programmed cell death 1 ligand 1 and tumor-infiltrating CD8+ T lymphocytes are prognostic factors of human ovarian cancer. *Proc. Natl. Acad. Sci. U. S. A. 104*, 3360−5.

(20) Hamid, O., Robert, C., Daud, A., Hodi, F. S., Hwu, W. J., Kefford, R., Wolchok, J. D., Hersey, P., Joseph, R. W., Weber, J. S., et al. (2013)

DOI: 10.1021/acs.bioconjchem.5b00318
Bioconjugate Chem. 2015, 26, 2062−2069

Safety and tumor responses with lambrolizumab (anti-PD-1) in melanoma. *N. Engl. J. Med. 369*, 134−44.
(21) Kim, P. S., and Ahmed, R. (2010) Features of responding T cells in cancer and chronic infection. *Curr. Opin. Immunol. 22*, 223−30.
(22) Mamalis, A., Garcha, M., and Jagdeo, J. (2014) Targeting the PD-1 pathway: a promising future for the treatment of melanoma. *Arch. Dermatol. Res. 306*, 511−9.
(23) Riley, J. L. (2009) PD-1 signaling in primary T cells. *Immunol. Rev. 229*, 114−25.
(24) Weber, J. S., Kudchadkar, R. R., Yu, B., Gallenstein, D., Horak, C. E., Inzunza, H. D., Zhao, X., Martinez, A. J., Wang, W., Gibney, G., et al. (2013) Safety, efficacy, and biomarkers of nivolumab with vaccine in ipilimumab-refractory or -naive melanoma. *J. Clin. Oncol. 31*, 4311−4318.
(25) Eisenhauer, E. A., Therasse, P., Bogaerts, J., Schwartz, L. H., Sargent, D., Ford, R., Dancey, J., Arbuck, S., Gwyther, S., Mooney, M., et al. (2009) New response evaluation criteria in solid tumours: revised RECIST guideline (version 1.1). *Eur. J. Cancer 45*, 228−47.
(26) Kurtz, D. M., and Gambhir, S. S. (2014) Tracking cellular and immune therapies in cancer. *Adv. Cancer Res. 124*, 257−96.
(27) Kaufman, H. L., Kirkwood, J. M., Hodi, F. S., Agarwala, S., Amatruda, T., Bines, S. D., Clark, J. I., Curti, B., Ernstoff, M. S., Gajewski, T., et al. (2013) The Society for Immunotherapy of Cancer consensus statement on tumour immunotherapy for the treatment of cutaneous melanoma. *Nat. Rev. Clin. Oncol. 10*, 588−98.
(28) Ahmadzadeh, M., Johnson, L. A., Heemskerk, B., Wunderlich, J. R., Dudley, M. E., White, D. E., and Rosenberg, S. A. (2009) Tumor antigen-specific CD8 T cells infiltrating the tumor express high levels of PD-1 and are functionally impaired. *Blood 114*, 1537−44.
(29) Chapon, M., Randriamampita, C., Maubec, E., Badoual, C., Fouquet, S., Wang, S. F., Marinho, E., Farhi, D., Garcette, M., Jacobelli, S., et al. (2011) Progressive upregulation of PD-1 in primary and metastatic melanomas associated with blunted TCR signaling in infiltrating T lymphocytes. *J. Invest. Dermatol. 131*, 1300−7.
(30) French, J. D., Kotnis, G. R., Said, S., Raeburn, C. D., McIntyre, R. C., Jr., Klopper, J. P., and Haugen, B. R. (2012) Programmed death-1+ T cells and regulatory T cells are enriched in tumor-involved lymph nodes and associated with aggressive features in papillary thyroid cancer. *J. Clin. Endocrinol. Metab. 97*, E934−43.
(31) Lee, C. M., and Tannock, I. F. (2010) The distribution of the therapeutic monoclonal antibodies cetuximab and trastuzumab within solid tumors. *BMC Cancer 10*, 255.
(32) Matsuzaki, J., Gnjatic, S., Mhawech-Fauceglia, P., Beck, A., Miller, A., Tsuji, T., Eppolito, C., Qian, F., Lele, S., Shrikant, P., et al. (2010) Tumor-infiltrating NY-ESO-1-specific CD8+ T cells are negatively regulated by LAG-3 and PD-1 in human ovarian cancer. *Proc. Natl. Acad. Sci. U. S. A. 107*, 7875−80.
(33) Muenst, S., Soysal, S. D., Gao, F., Obermann, E. C., Oertli, D., and Gillanders, W. E. (2013) The presence of programmed death 1 (PD-1)-positive tumor-infiltrating lymphocytes is associated with poor prognosis in human breast cancer. *Breast Cancer Res. Treat. 139*, 667−76.
(34) Scott, A. M., Wolchok, J. D., and Old, L. J. (2012) Antibody therapy of cancer. *Nat. Rev. Cancer 12*, 278−87.
(35) Sfanos, K. S., Bruno, T. C., Meeker, A. K., De Marzo, A. M., Isaacs, W. B., and Drake, C. G. (2009) Human prostate-infiltrating CD8+ T lymphocytes are oligoclonal and PD-1+. *Prostate 69*, 1694−703.
(36) Sun, S., Fei, X., Mao, Y., Wang, X., Garfield, D. H., Huang, O., Wang, J., Yuan, F., Sun, L., Yu, Q., et al. (2014) PD-1(+) immune cell infiltration inversely correlates with survival of operable breast cancer patients. *Cancer Immunol. Immunother. 63*, 395−406.
(37) Zhang, Y., Huang, S., Gong, D., Qin, Y., and Shen, Q. (2010) Programmed death-1 upregulation is correlated with dysfunction of tumor-infiltrating CD8+ T lymphocytes in human non-small cell lung cancer. *Cell. Mol. Immunol. 7*, 389−95.
(38) Shi, F., Shi, M., Zeng, Z., Qi, R. Z., Liu, Z. W., Zhang, J. Y., Yang, Y. P., Tien, P., and Wang, F. S. (2011) PD-1 and PD-L1 upregulation promotes CD8(+) T-cell apoptosis and postoperative recurrence in hepatocellular carcinoma patients. *Int. J. Cancer 128*, 887−96.
(39) Taube, J. M., Klein, A., Brahmer, J. R., Xu, H., Pan, X., Kim, J. H., Chen, L., Pardoll, D. M., Topalian, S. L., and Anders, R. A. (2014) Association of PD-1, PD-1 ligands, and other features of the tumor immune microenvironment with response to anti-PD-1 therapy. *Clin. Cancer Res. 20*, 5064−74.
(40) Grosso J, H. C., Inzunza, D., Cardone, D. M., Simon, J. S., and Gupta, A. K. (2013) Association of tumor PD-L1 expression and immune biomarkers with clinical activity in patients with advanced solid tumors treated with nivolumab. *Journal of Clinical Oncology 31*, 3016.
(41) Herbst, R. S., Gordon, M. S., Fine, G. D., Sosman, J. A., Soria, J. C., and Hamid (2013) A study of MPDL3280A, an engineered PD-L1 antibody in patients with locally advanced or metastatic tumors. *Journal of Clinical Oncology 31*, 3000.
(42) Suffner, J., Hochweller, K., Kuhnle, M. C., Li, X., Kroczek, R. A., Garbi, N., and Hammerling, G. J. (2010) Dendritic cells support homeostatic expansion of Foxp3+ regulatory T cells in Foxp3.LuciDTR mice. *J. Immunol. 184*, 1810−20.
(43) Zhou, Q., Munger, M. E., Highfill, S. L., Tolar, J., Weigel, B. J., Riddle, M., Sharpe, A. H., Vallera, D. A., Azuma, M., Levine, B. L., et al. (2010) Program death-1 signaling and regulatory T cells collaborate to resist the function of adoptively transferred cytotoxic T lymphocytes in advanced acute myeloid leukemia. *Blood 116*, 2484−93.
(44) Sage, P. T., Francisco, L. M., Carman, C. V., and Sharpe, A. H. (2012) The receptor PD-1 controls follicular regulatory T cells in the lymph nodes and blood. *Nat. Immunol. 14*, 152−61.
(45) Lipson, E. J., Sharfman, W. H., Drake, C. G., Wollner, I., Taube, J. M., Anders, R. A., Xu, H., Yao, S., Pons, A., Chen, L., et al. (2013) Durable cancer regression off-treatment and effective reinduction therapy with an anti-PD-1 antibody. *Clin. Cancer Res. 19*, 462−8.
(46) Natarajan, A., and Gambhir, S. S. (2015) Radiation Dosimetry Study of [(89)Zr]rituximab Tracer for Clinical Translation of B cell NHL Imaging using Positron Emission Tomography. *Mol. Imaging Biol. 17*, 539.
(47) Lindmo, T., Boven, E., Cuttitta, F., Fedorko, J., and Bunn, P. A., Jr. (1984) Determination of the immunoreactive fraction of radiolabeled monoclonal antibodies by linear extrapolation to binding at infinite antigen excess. *J. Immunol. Methods 72*, 77−89.

DOI: 10.1021/acs.bioconjchem.5b00318
Bioconjugate Chem. 2015, 26, 2062−2069